FRONTIERS OF PHYSICS

RESEARCH ARTICLE
Volume 21 / Issue 8 / 085207 / 2026

Time reversal preserved spin valve and spin transistor based on unconventional *p*-wave magnets

Ze-Yong Yuan[1], Jun-Feng Liu[1,†], Pei-Hao Fu[1,‡], Jun Wang[2,§]

1 School of Physics and Materials Science, Guangzhou University, Guangzhou 510006, China
2 Department of Physics, Southeast University, Nanjing 210096, China
Corresponding authors. E-mail: †phjfliu@gzhu.edu.cn, ‡phy.phfu@gmail.com, §jwang@seu.edu.cn
Received December 23, 2025; accepted April 24, 2026

ABSTRACT

The anisotropic spin splitting in unconventional magnets opens new opportunities for realizing spintronic functionalities without relying on net magnetization or relativistic spin–orbit coupling. Here, we propose a spin valve and a spin transistor based on unconventional *p*-wave magnets (UPMs). The spin valve is realized in a junction where a normal metal is sandwiched between two UPMs whose exchange-field strength vectors are oriented transverse to the junction direction. The conductance of such a device is governed by the spin alignment between two UPMs: when their strength vectors are parallel, the spin-state alignment enables efficient electron transmission, leading to a high-conductance state; in contrast, the antiparallel configuration suppresses the conductance owing to the opposite spin orientations. Furthermore, the spin-valve can be extended to a spin transistor by replacing the central normal metal with another UPM with a longitudinally oriented strength vector and a perpendicular spin polarization axis. The central UPM enables uniform spin precession with the same precession frequency for all transverse modes. Both devices can be electrically controlled by modulating the strength vectors of UPMs. These findings establish UPMs as a promising platform for developing spintronic devices without net magnetization or relativistic spin–orbit coupling.

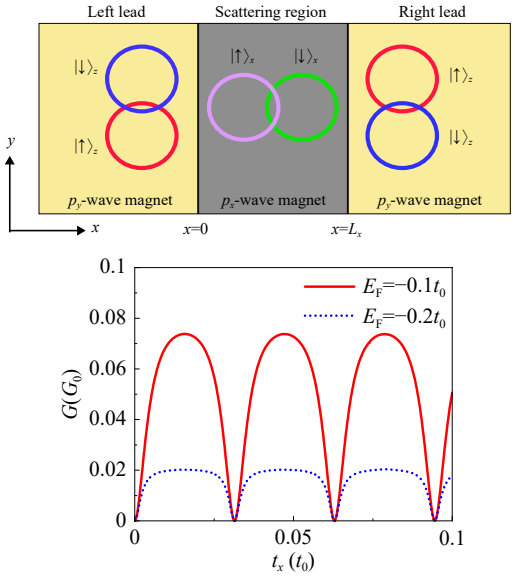

Keywords spin valve, spin transistor, unconventional *p*-wave magnets

1 Introduction

Unconventional magnets (UMs) [1–11] represent the third distinct magnetic phase that breaks the traditional dichotomy between ferromagnetism [12] and antiferromagnetism [13]. UMs are characterized by a directional spin-split Fermi surface that lifts the spin degeneracy analogously to ferromagnets while maintaining vanishing net magnetization in antiferromagnets. Based on the symmetry of the Fermi surface in momentum space, UMs are classified into two categories [9]: even–parity magnetic orders (e.g., d-, g-, and i-wave types) [7, 10] and odd–parity magnetic orders (e.g., p-, f- and h-wave types) [6, 14–16]. Even-parity magnetic order, corresponding to the degree $\ell = 0, 2, 4,$ or 6 of the exchange magnetic field polynomials with momentum space as variables, breaks time-reversal symmetry while preserving inversion symmetry. This results in spin-split energy bands that satisfy $E_\sigma(\boldsymbol{k}) = E_\sigma(-\boldsymbol{k})$ but $E_\sigma(\boldsymbol{k}) \neq E_{-\sigma}(\boldsymbol{k})$. In contrast, odd-parity magnetic orders, corresponding

*Special Topic: Altermagnets: Exploring New Physical Phenomena and Effects (Editor: Sandong Guo).

Higher Education Press

https://doi.org/10.15302/frontphys.2026.085207

to the degree $\ell = 1, 3$, or 5 of the exchangemagnetic field in momentum, preserve time-reversal symmetry but break inversion symmetry. Their band structure is characterized by the relations $E_\sigma(\boldsymbol{k}) \neq E_\sigma(-\boldsymbol{k})$ and $E_\sigma(\boldsymbol{k}) = E_{-\sigma}(-\boldsymbol{k})$ [9, 17].

In altermagnets, the even–parity spin splitting underlies a variety of spintronic and transport phenomena [4, 5], including giant magnetoresistance [18], spin-transfer torques [19–21], spin filtering [22–24], spin precession and spin transistor [25], spin pumping effects [26], nonlinear transports [27], light–matter interactions [28–31], magneto-optical effects [32], light-induced spin density [30, 31], non-Hermitian electronic responses [33, 34], strongly correlation in Mott insulators [35] and other novel phenomena [36–50, 50–56]. With all the above-mentioned developments in both theory and experiments [57–65], altermagnets have been established as a versatile platform for generating and manipulating spin currents [26, 66–72], which can be realized in a wide range of representative candidate materials include RuF_4 [73], MnTe [74, 75], $CoNb_3S_6$ [76], and RuO_2 [77], although its altermagnetic nature is still under debate [78–81].

Research on odd–parity unconventional magnets remains comparatively less explored, compared to their well-developed even–parity counterparts discussed above. Particularly, UMs with p-wave symmetry, referred to as unconventional p-wave magnets (UPMs) [10], exhibit momentum-dependent spin splitting and nonrelativistic spin–momentum locking. Thus, by effectively mimicking spin–orbit coupling [82, 83] and preserving time-reversal symmetry, UPMs provide an appealing platform for scalable spintronic applications [4, 84–86]. Extensive efforts have been devoted to exploring their normal-state properties [87–90], including tunneling magnetoresistance [15, 91], orientation-dependent anomalous Hall effects [92], spin-current generation [17], and non-Hermitian responses [93, 94]. Their superconducting counterparts have also attracted considerable attention, revealing rich phenomena such as tunneling spin Hall effects [95], transverse spin supercurrents [96], and orientation-dependent transport in UPM-superconductor hybrids [43, 97–100], among other phenomena [89, 99, 101]. On the materials side, UPMs have been theoretically proposed in compounds such as Mn_3GaN and CeNiAsO [6], and very recent experiments have reported their realization in thin flakes of NiI_2 [102] and metallic $Gd_3Ru_4Al_{12}$ [103]. Notably, the demonstrated ability to electrically switch the Néel vector in UPMs [104, 105] further underscores their potential for spintronic memory applications [102].

Despite the above-mentioned advances, proposals for spintronic devices directly leveraging p-wave magnets remain largely unexplored. Two prototypical spintronic architectures, the spin valve [106, 107] and the spin field-effect transistor (SFET) [108–110], offer ideal testbeds for realizing nonrelativistic, time-reversal-symmetric spin

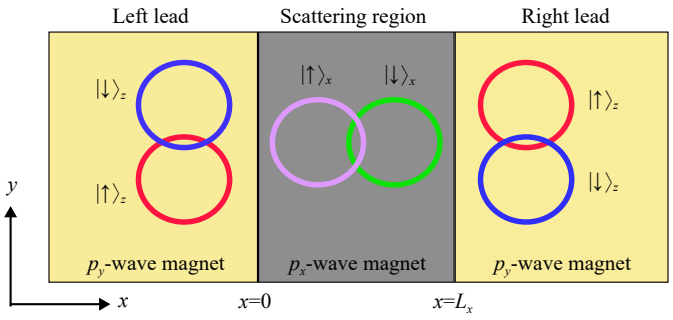

Fig. 1 Schematic of a UPM/UPM/UPM junction. In the left and right leads, the strength vectors of two UPMs are along the y direction, inducing a splitting of the Fermi surface along the k_y direction. And the spin polarization is along the z direction. In the central UPM, the strength vector is along the x direction and the spin polarization is along the x direction, enabling a spin precession.

control. In a conventional spin valve [106, 107], two ferromagnetic layers can be tuned between parallel (P) and antiparallel (AP) magnetization states: conduction occurs only for spins aligned with the local magnetization, leading to high conductance in the P configuration and suppression in the AP configuration. Switching between P and AP states typically requires an external magnetic field [23]. In contrast, an SFET exploits spin precession [108–110]: as electrons travel through the channel, their spins precess due to spin–orbit coupling, and a gate voltage modulates the precession frequency, thereby controlling the conductance. Such devices leverage the spin degree of freedom for information processing and storage, promising low power consumption, high speed, and dense integration [106, 108].

In this work, we propose a *time-reversal-symmetric* spin valve and a spin transistor based on UPMs. As illustrated in Fig. 1, the junction functions as a spin valve when the two UPM electrodes possess transverse exchange-field strength vectors and the central region acts as a normal metal (zero exchange-field strength). Under AP alignment, the conductance is strongly suppressed at low Fermi energies, whereas P alignment restores finite conductance. This arises from the anisotropic spin splitting of the Fermi surfaces along the transverse direction: when the Fermi contours on both sides are fully separated in the momentum space, the junction behaves as an ideal spin valve. Moreover, replacing the central normal region with another UPM whose strength vector points longitudinally perpendicular to those in the electrodes converts the device into a spin transistor. The longitudinally split Fermi surface induces coherent spin precession across all transverse momenta, leading to oscillatory conductance analogous to the Datta-Das mechanism [111]. Since the magnitude and orientation of the UPM strength vectors can be effectively controlled via electrically tuning of the spin polarization

[102], the proposed spin valves and spin transistors provide a fully nonrelativistic route toward spintronic functionality without net magnetization or spin–orbit coupling. The well-separated Fermi surfaces of UPMs, a feature also observed in other unconventional magnets [18], facilitate high-contrast switching in spin valves. Compared with other unconventional magnets, the global shift of Fermi surfaces in UPMs allows for perfect spin precession in spin transistors.

2 Model and methods

As a unified model for a spin valve and a spin transistor, we consider a UPM/UPM/UPM trilayer junction, as shown in Fig. 1. For the left and right UPM leads, the strength vectors are along the y direction and the spin polarization is along the z direction. For the central UPM, the strength vector is along the x direction and the spin polarization is along the x direction. The tight-binding Hamiltonian for the junction is given by [17]

$$\begin{aligned} H = & -t_0 \sum_{\boldsymbol{j}} \left(C_{\boldsymbol{j}}^{\dagger} C_{\boldsymbol{j}+\hat{x}} + C_{\boldsymbol{j}}^{\dagger} C_{\boldsymbol{j}+\hat{y}} + \text{h.c.} \right) + 4t_0 \\ & + \sum_{\boldsymbol{j}} \left\{ \mathrm{i} t_x [\Theta(x) - \Theta(x - L_x)] C_{\boldsymbol{j}}^{\dagger} \sigma_x C_{\boldsymbol{j}+\hat{x}} + \text{h.c.} \right\} \\ & + \sum_{\boldsymbol{j}} \left\{ \mathrm{i} [t_{yL} \Theta(-x) + t_{yR} \Theta(x - L_x)] C_{\boldsymbol{j}}^{\dagger} \sigma_z C_{\boldsymbol{j}+\hat{y}} + \text{h.c.} \right\} \\ & + U_0 \sum_{\boldsymbol{j}} [\Theta(x) - \Theta(x - L_x)] C_{\boldsymbol{j}}^{\dagger} C_{\boldsymbol{j}} + \gamma \sum_{j_x \in \{0, L_x\}, j_y} C_{\boldsymbol{j}}^{\dagger} C_{\boldsymbol{j}}, \end{aligned} \tag{1}$$

where $C_{\boldsymbol{j}}^{\dagger} = (C_{\boldsymbol{j}\uparrow}^{\dagger}, C_{\boldsymbol{j}\downarrow}^{\dagger})$ are electron creation operators, $\boldsymbol{j} = (j_x, j_y)$ denotes the lattice coordinates, $\hat{x}$ ($\hat{y}$) is the unit vector in the x (y) direction, and $\Theta(x)$ is the step function. Here t_0 denotes the nearest-neighbor hopping energy, t_{yL} (t_{yR}) is the magnitude of the strength vector along the y direction in the left (right) UPM lead, and t_x is the magnitude of the strength vector along the x direction in the central UPM. σ_x and σ_z are Pauli matrices in spin space. U_0 is the on-site energy in the central UPM region, and γ represents the strength of the interfacial barriers.

For simplicity, the translational symmetry along the y direction is assumed to be preserved and the transverse momentum k_y is conserved. Within the Landauer–Büttiker formalism, the conductance at a fixed Fermi energy E_F is expressed in terms of the total transmission probability $T(k_y, E_F)$ [112],

$$G = G_0 \int T(E_F, k_y) \mathrm{d}k_y, \tag{2}$$

where $G_0 = 2e^2 L_y/(2\pi h)$, L_y is the width of the system. The transmission probability can be calculated by the lattice Green function technique [23, 113–115]

$$T(k_y, E_F) = \mathrm{Tr}\left(\Gamma_L G^r \Gamma_R G^a\right). \tag{3}$$

Here,

$$\Gamma_{L/R} = \mathrm{i}\left[\Sigma_{L/R}^r - (\Sigma_{L/R}^r)^{\dagger}\right] \tag{4}$$

are the linewidth functions. The retarded Green function is

$$G^r(E) = [E - H_C - \Sigma_L^r(E) - \Sigma_R^r(E)]^{-1} \tag{5}$$

and $G^a = [G^r(E)]^{\dagger}$, where H_C is the Hamiltonian of the central UPM, the retarded self-energies $\Sigma_{L/R}^r(E)$ representing the coupling with the leads can be calculated numerically by the recursive method [116].

In the following section, we investigate the conductance of the junction illustrated in Fig. 1 and its dependence on key parameters, including Fermi energy E_{F}, UPM strength t_x, junction length L_x, and interfacial barrier γ. By incorporating insights from the Fermi surface, dispersion relations, and conductance modulation mechanisms, we examine the conditions for realizing spin valves and spin transistors based on UPM junctions.

3 Results and discussion

In this section, we propose two electrically controlled spintronic devices that utilize the anisotropic spin splitting of UPMs: a spin valve (see Fig. 2) and a spin transistor (see Figs. 3 and 4). The dependence of the conductance on the strength vectors and the spin polarizations of UPMs enables tunable spin and charge transport in UPM-based junctions, offering a promising platform for zero-net-magnetization spintronic applications.

We start by considering the Hamiltonians of three regions of the device. By applying Fourier transforms, the low-energy Hamiltonian for the left and right leads in the momentum space can be obtained as

$$H_{L/R}(\boldsymbol{k}) = t_0(k_x^2 + k_y^2) + 2t_{yL/R} k_y \sigma_z, \tag{6}$$

where $t_{yL/R}$ denotes the strength of p_y-wave magnetization in the left (right) lead and the lattice constant is set as $a = 1$. The Hamiltonian for the central UPM is

$$H_C(\boldsymbol{k}) = t_0(k_x^2 + k_y^2) + 2t_x k_x \sigma_x + U_0. \tag{7}$$

Note that the exchange field in UPMs can be consistently defined as $(\boldsymbol{t} \cdot \boldsymbol{k})\boldsymbol{\sigma} \cdot \boldsymbol{n}$, where $\boldsymbol{t}$ denotes the strength vector and $\boldsymbol{n}$ represents the spin polarization vector.

The spin-resolved band structures for the two UPM leads can be found as

$$E_{L/R} = t_0 \left[k_x^2 + (k_y + \sigma \alpha_{yL/R})^2 - \alpha_{yL/R}^2\right], \tag{8}$$

where $\alpha_{yL/R} = t_{yL/R}/t_0$, and $\sigma = 1(-1)$ for the spin-up (-down) subband with respect to the z direction. For the

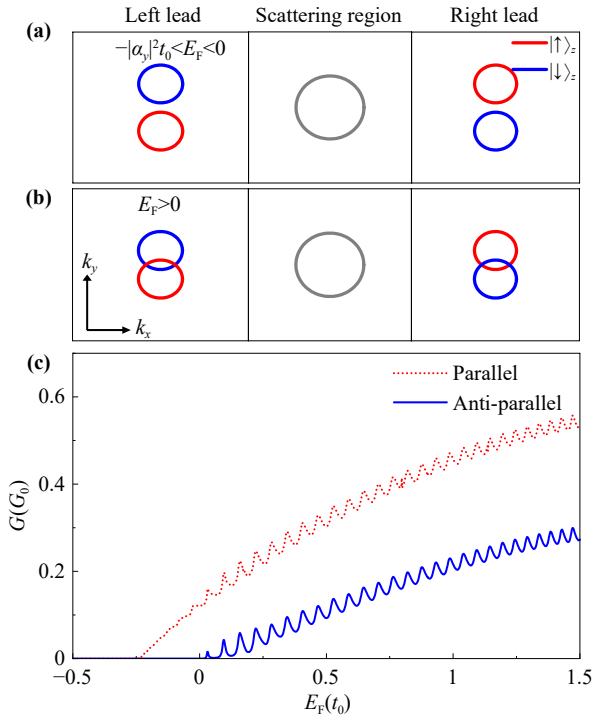

Fig. 2 **(a, b)** Spin-split Fermi circles in two leads for the antiparallel configuration at negative and positive Fermi energies, respectively. **(c)** The conductance as the function of the Fermi energy of the UPM-based spin valve in the parallel and antiparallel configurations. The parameters used are as follows: $\alpha_{yL} = 0.5$, $\alpha_{yR} = -\alpha_{yL}$, $\alpha_y = |\alpha_{yL}| = |\alpha_{yR}|$, $U_0 = -2t_0$, $L_x = 100a$, with $a = 1$ the lattice constant and $t_0 = 1$ the energy unit.

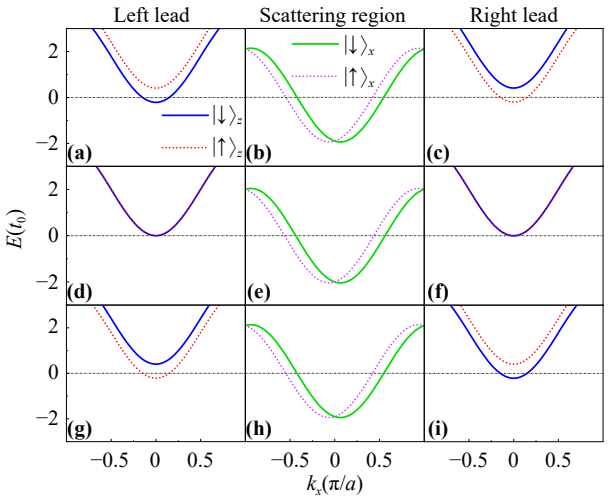

Fig. 3 Spin-split subbands in the three regions of the UPM-based SFET in the antiparallel configuration of two leads. Panels **(a)**–**(c)**, **(d)**–**(f)**, and **(g)**–**(i)** correspond to $k_y = 0.1\pi/a$, $k_y = 0$, and $k_y = -0.1\pi/a$, respectively. Different colors correspond to distinct spin orientations. The parameters used are as follows: $U_0 = -2t_0$, $t_{yL} = 0.5t_0$, $t_{yR} = -0.5t_0$, $t_x = 0.2t_0$.

central UPM, the band dispersion is

$$E_C = t_0 \left[(k_x + \sigma'\alpha_x)^2 + k_y^2 - \alpha_x^2\right] + U_0, \tag{9}$$

where $\alpha_x = t_x/t_0$, and $\sigma' = 1(-1)$ for the spin-up (-down) subband with respect to the x direction.

First, we consider a UPM/normal-metal/UPM junction which acts as a spin valve. To model the central region as a normal metal, we set $t_x = 0$. According to Eq. (8), the left and right leads exhibit spin-split Fermi circles at a fixed Fermi energy E_F, with the splitting occurring along the k_y direction, as illustrated in Figs. 2(a) and (b). When $E_F > 0$, the two spin-split Fermi circles still overlap. In contrast, for $E_F < 0$, two circles become completely separated. It is important to note that both the transverse momentum k_y and the spin component σ_z are conserved during transport when $t_x = 0$. Consequently, a transport channel opens only when both k_y and the spin state are matched between the two leads.

We examine both parallel ($t_{yR} = t_{yL}$) and antiparallel ($t_{yR} = -t_{yL}$) configurations of the strength vectors in the two UPM leads. In the antiparallel configuration, when the Fermi energy lies within the interval $E_F \in (-\alpha_y^2 t_0, 0)$, with $\alpha_y = |\alpha_{yL}| = |\alpha_{yR}|$, the two Fermi circles are spin-split in opposite directions along the k_y axis and are fully separated, as shown in Fig. 2(a). For a fixed k_y, the spin orientations in the two leads are opposite. This spin mismatch prevents the opening of any transport channel. Incident electrons from the left lead are thus completely reflected, resulting in zero conductance, as depicted in Fig. 2(c). However, when $E_F > 0$, a partial overlap occurs between two spin-split Fermi circles in both leads, as shown in Fig. 2(b). Within this overlapping k_y region, both spin-up and spin-down states are available in both leads, allowing transport channels to open and yielding a non-zero conductance. As the Fermi energy increases, the overlap area of the Fermi circles expands, leading to a general increase in conductance, albeit with slight oscillations caused by multiple reflections at the interfaces [23, 24].

Conversely, in the parallel configuration, the Fermi circles in both leads are split in the same direction along the k_y axis. For any given k_y, the spin states are identical in both leads. Transport channels are open whenever the Fermi energy is above the bottom of the subbands, i.e., $E_F > -\alpha_y^2 t_0$. The significant contrast in conductance between the antiparallel and parallel configurations within the energy range $E_F \in (-\alpha_y^2 t_0, 0)$ enables a high on/off ratio in this UPM-based spin valve, which can be electrically controlled by tuning the strength vectors of the leads.

Unlike conventional ferromagnetic spin valves [106, 107], the proposed UPM spin valve exhibits zero net magnetization. Its conductance is governed by the relative alignment of the UPMs' strength vectors rather than macroscopic magnetizations. More importantly, switching

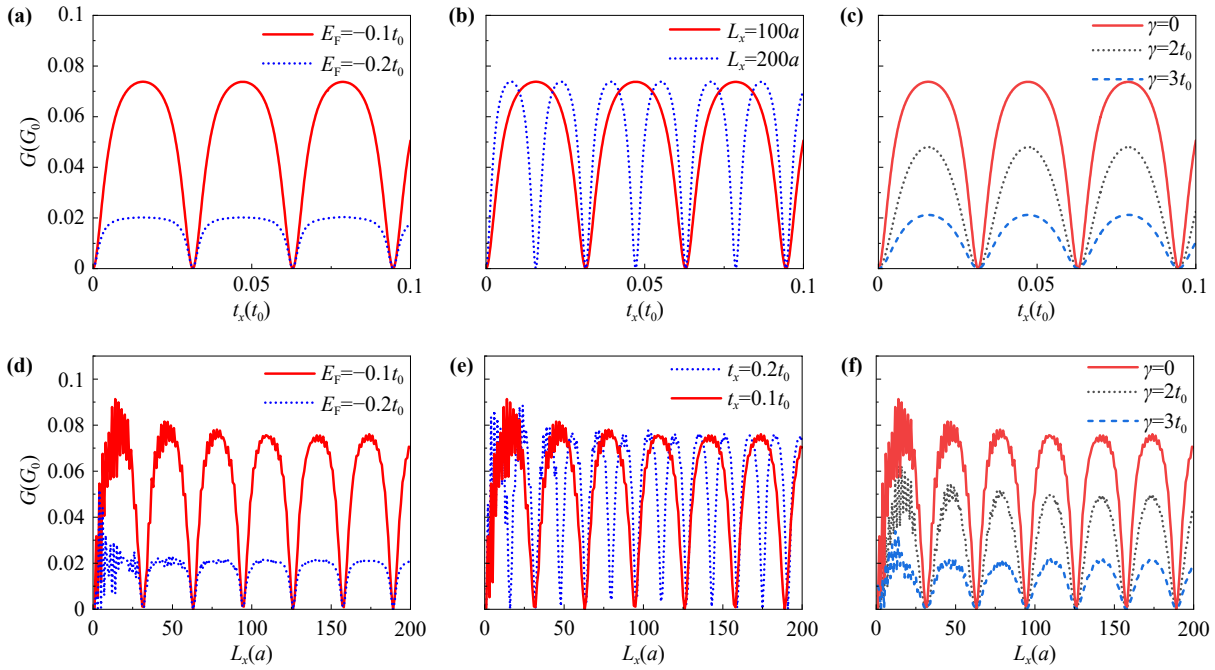

Fig. 4 Conductance oscillations versus t_x and L_x at negative Fermi energies in the SFET. Parameters for (b) and (e): $E_F = -0.1t_0$; for (c) and (f): $E_F = -0.1t_0$, $L_x = 100a$, $t_x = 0.1t_0$; for **(a–f)**: $U_0 = -2t_0$.

between parallel and antiparallel configurations in conventional spin valves typically requires an external magnetic field to reverse the magnetization of one ferromagnetic lead. In contrast, switching in our UPM-based spin valve is achieved by electrically tuning the strength vectors, offering a more practical control mechanism.

Second, we consider a UPM/UPM/UPM junction functioning as a SFET. Here, the central normal metal is replaced by a UPM whose strength vector and spin quantum axis are both along the x direction. The perpendicular orientation of this spin axis relative to those in the leads, combined with the longitudinally split Fermi circles (see Fig. 1), enables spin precession for incident electrons traversing the central region. Based on the tight-binding Hamiltonians, we plot the spin-split band dispersions for each region of the SFET in Fig. 3, illustrating the preserved time-reversal symmetry. In the antiparallel configuration with $E_F < 0$, the spins of the occupied subbands are opposite in the two leads, which would result in zero conductance in a simple spin valve junction. However, the inclusion of the central p_x-wave UPM, with its longitudinally split subbands and perpendicular spin axis (see Fig. 3), induces spin precession. According to Eq. (9), the wave vector difference is $\Delta k_x = 2\alpha_x$, leading to a precession angle of $2\alpha_x L_x$. The conductance reaches a maximum [108] when $2\alpha_x L_x = (2n+1)\pi$ and drops to zero when $2\alpha_x L_x = 2n\pi$, where n is an integer.

Figure 4 demonstrates periodic oscillations in conductance as a function of the UPM strength t_x and the length L_x of the central region. For $E_F < 0$, the conductance minima can reach zero due to perfect spin precession within the central UPM. A key advantage is that the wave vector difference $\Delta k_x = 2\alpha_x$ remains constant for all transverse modes k_y, a consequence of the longitudinal spin-splitting along the k_x direction. This uniformity ensures that all transverse modes precess at the same frequency, allowing their transmissions to vanish simultaneously and resulting in a true zero conductance state – a crucial feature for a high-performance SFET with a high on/off ratio. This behavior contrasts with the original Datta–Das transistor based on Rashba spin-orbit coupling [111], where differing precession frequencies for different transverse modes prevent the conductance from reaching zero in the off state. As shown in Fig. 4(b), doubling the length L_x halves the oscillation period of the conductance versus t_x, which is consistent with the spin precession analysis. Notably, t_x can be tuned effectively by modulating the spin polarization via an external electric field [102], providing electrical control of the SFET.

In addition to the primary spin precession oscillations, the conductance versus L_x also exhibits minor oscillations due to multiple reflections at the interfaces, as shown in Figs. 4(d)–(f). These resonance transmission induced oscillations are absent in the dependence versus t_x dependence because varying t_x simultaneously alters both the right-going and left-going wave vectors by the same amount, leaving the resonant conditions relatively unaffected.

Finally, we examine the effect of interfacial barriers on the performance of SFET. Figures 4(c) and (f) show

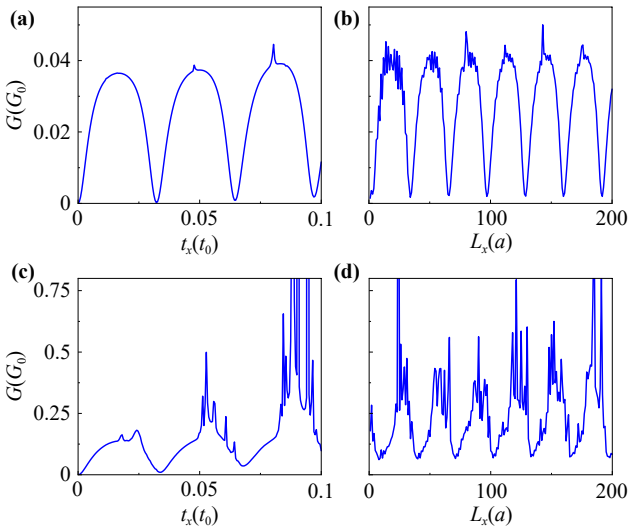

Fig. 5 Influence of two buffer layers at interfaces on the conductance of the SFET. **(a)** and **(b)** show the conductance for a buffer layer with width $L_n = 3a$, while **(c)** and **(d)** correspond to $L_n = 10a$, where a is the lattice constant. The other parameters are set as follows: for (a) and (c), $L_x = 100a$; for (b) and (d), $t_x = 0.1t_0$; and $E_F = -0.1t_0$ for all subfigures.

the conductance for varying barrier strength γ. While stronger interfacial barriers reduce the maximum conductance, they also smoothen the conductance minima, which can enhance the practical tunability of the device. The introduction of elastic impurities in the central scattering region produces an effect similar to that of interfacial barriers on the conductance, leading to a moderate suppression of the conductance maxima and a concomitant smoothing of the conductance minima, with results analogous to those presented in Figs. 4(c) and (f).

To facilitate spin polarization control in a specific layer of the heterostructure and to mitigate the influence of the local electric field on neighboring layers, we insert buffer layers of width L_n between the central scattering region and the two leads. As shown in Fig. 5, the conductance depends distinctly on the buffer layer width. For a narrow buffer (e.g., $L_n = 3a$), the maximum conductance is lower than in the no-buffer case, yet a high on/off ratio is maintained. This indicates that even a narrow buffer can effectively suppress interlayer interference. In contrast, a wider buffer (e.g., $L_n = 10a$) substantially increases the conductance, enhancing the on-state performance at the cost of a slightly reduced on/off ratio. These results demonstrate that the buffer layer design offers a tunable means to balance the minimization of interlayer crosstalk against the optimization of conductance. It thereby alleviates the difficulty of selectively tuning spin polarization in a target layer while containing the impact of local electric fields on adjacent regions.

4 Conclusion

This work proposes two core spintronic devices, a spin valve and a spin transistor, based on UPMs. Both devices operate under time-reversal symmetry and require neither net magnetization nor relativistic spin-orbit coupling, offering a distinct mechanism for spin manipulation. The spin valve effect is achieved by electrically switching the strength vectors of two UPM electrodes between parallel and antiparallel configurations. Conductance is suppressed in the antiparallel state when two Fermi circles separate in momentum space, yielding a high on/off ratio. Replacing the central normal region with an orthogonally polarized UPM converts the device into a spin transistor. The longitudinal spin-splitting in the central region enables uniform spin precession for all transverse modes, leading to full-conductance oscillations and a perfectly modulated on/off state – a key advantage over conventional spin–orbit-coupled transistors. Electrical tunability of the UPM strength vectors allows active control of conductance, as demonstrated by oscillation periods dependent on t_x and L_x. Supported by recent experiments on electrical switching in UPMs, these findings establish UPMs as an integrable platform for low-power, magnetic-field-free spintronic applications [102].

Declarations The authors declare that they have no competing interests and there are no conflicts.

Data availability The data supporting the findings of this study are available from the corresponding authors upon reasonable request.

Acknowledgements The work described in this paper was supported by the National Natural Science Foundation of China (Grant Nos. 12174077 and 12174051).

References

1. S. Shim, M. Mehraeen, J. Sklenar, S. S. L. Zhang, A. Hoffmann, and N. Mason, Spin-polarized antiferromagnetic metals, *Annu. Rev. Condens. Matter Phys.* 16(1), 103 (2025)
2. S. W. Cheong and F. T. Huang, Altermagnetism classification, *npj Quantum Mater.* 10(1), 38 (2025)
3. T. Jungwirth, R. M. Fernandes, J. Sinova, and L. Smejkal, Altermagnets and beyond: Nodal magnetically-ordered phases, arXiv: 2409.10034 (2024)
4. L. Bai, W. Feng, S. Liu, L. Smejkal, Y. Mokrousov, and Y. Yao, Altermagnetism: Exploring new frontiers in magnetism and spintronics, *Adv. Funct. Mater.* 34(49), 2409327 (2024)
5. H. Yan, X. Zhou, P. Qin, and Z. Liu, Review on spin-split antiferromagnetic spintronics, *Appl. Phys. Lett.* 124(3), 030503 (2024)
6. A. B. Hellenes, T. Jungwirth, R. Jaeschke-Ubiergo, A. Chakraborty, J. Sinova, and L. Šmejkal, *P*-wave magnets, arXiv: 2309.01607 (2024)

7. L. Šmejkal, J. Sinova, and T. Jungwirth, Beyond conventional ferromagnetism and antiferromagnetism: A phase with nonrelativistic spin and crystal rotation symmetry, *Phys. Rev. X* 12(3), 031042 (2022)
8. T. Jungwirth, R. M. Fernandes, E. Fradkin, A. H. MacDonald, J. Sinova, and L. Šmejkal, Altermagnetism: An unconventional spin-ordered phase of matter, *Newton* 1(6), 100162 (2025)
9. Y. Fukaya, B. Lu, K. Yada, Y. Tanaka, and J. Cayao, Superconducting phenomena in systems with unconventional magnets, *J. Phys. : Condens. Matter* 37(31), 313003 (2025)
10. L. Šmejkal, J. Sinova, and T. Jungwirth, Emerging research landscape of altermagnetism, *Phys. Rev. X* 12(4), 040501 (2022)
11. S. Zeng, D. Liu, H. Peng, C. C. He, X. B. Yang, and Y. J. Zhao, Classification and design of two-dimensional altermagnets, *Front. Phys. (Beijing)* 21(9), 095301 (2026)
12. L. Néel, Magnetism and local molecular field, *Science* 174(4013), 985 (1971)
13. L. Néel, Some new results on antiferromagnetism and ferromagnetism, *Rev. Mod. Phys.* 25(1), 58 (1953)
14. Y. B. Kudasov, Topological band structure due to modified Kramers degeneracy for electrons in a helical magnetic field, *Phys. Rev. B* 109(14), L140402 (2024)
15. B. Brekke, P. Sukhachov, H. G. Giil, A. Brataas, and J. Linder, Minimal models and transport properties of unconventional p-wave magnets, *Phys. Rev. Lett.* 133(23), 236703 (2024)
16. Y. Yu, M. B. Lyngby, T. Shishidou, M. Roig, A. Kreisel, M. Weinert, B. M. Andersen, and D. F. Agterberg, Odd-parity magnetism driven by antiferromagnetic exchange, *Phys. Rev. Lett.* 135(4), 046701 (2025)
17. A. A. Hedayati and M. Salehi, Transverse spin current at normal-metal/p-wave magnet junctions, *Phys. Rev. B* 111(3), 035404 (2025)
18. L. Šmejkal, A. B. Hellenes, R. González-Hernández, J. Sinova, and T. Jungwirth, Giant and tunneling magnetoresistance in unconventional collinear antiferromagnets with nonrelativistic spin-momentum coupling, *Phys. Rev. X* 12(1), 011028 (2022)
19. H. Bai, L. Han, X. Y. Feng, Y. J. Zhou, R. X. Su, Q. Wang, L. Y. Liao, W. X. Zhu, X. Z. Chen, F. Pan, X. L. Fan, and C. Song, Observation of spin splitting torque in a collinear antiferromagnet RuO_2, *Phys. Rev. Lett.* 128(19), 197202 (2022)
20. S. Karube, T. Tanaka, D. Sugawara, N. Kadoguchi, M. Kohda, and J. Nitta, Observation of spin-splitter torque in collinear antiferromagnetic RuO2, *Phys. Rev. Lett.* 129(13), 137201 (2022)
21. S. Han, D. Jo, I. Baek, S. Cheon, P. M. Oppeneer, and H. W. Lee, Harnessing magnetic octupole Hall effect to induce torque in altermagnets, *Phys. Rev. Lett.* 135(7), 076705 (2025)
22. K. Samanta, D. F. Shao, and E. Y. Tsymbal, Spin filtering with insulating altermagnets, *Nano Lett.* 25(8), 3150 (2025)
23. P. H. Fu, Q. Lv, Y. Xu, J. Cayao, J. F. Liu, and X. L. Yu, All-electrically controlled spintronics in altermagnetic heterostructures, *npj Quantum Mater.* 10(1), 111 (2025)
24. Q. Lv, Y. Xu, J. F. Liu, P. H. Fu, and X. L. Yu, Gate engineering Fabry–Pérot resonance in altermagnetic junctions, *Sci. Rep.* 15(1), 45508 (2025)
25. L. S. Liu, K. Shao, H. D. Li, X. Wan, W. Chen, and D. Y. Xing, Altermagnetic spin precession and spin transistor, *Phys. Rev. Lett.* 136(10), 106301 (2026)
26. C. Sun and J. Linder, Spin pumping from a ferromagnetic insulator into an altermagnet, *Phys. Rev. B* 108(14), L140408 (2023)
27. H. Zhu, J. Li, X. Chen, Y. Yu, and Q. Liu, Magnetic geometry induced quantum geometry and nonlinear transports, *Nat. Commun.* 16(1), 4882 (2025)
28. P. Werner, M. Lysne, and Y. Murakami, High harmonic generation in altermagnets, *Phys. Rev. B* 110(23), 235101 (2024)
29. T. Farajollahpour, R. Ganesh, and K. V. Samokhin, Light-induced charge and spin Hall currents in materials with $C4K$ symmetry, *npj Quantum Mater.* 10(1), 29 (2025)
30. P. H. Fu, S. Mondal, J. F. Liu, Y. Tanaka, and J. Cayao, Floquet Engineering Spin Triplet States in Unconventional Magnets, *Phys. Rev. Lett.* 136(6), 066703 (2026)
31. P. H. Fu, S. Mondal, J. F. Liu, and J. Cayao, Light-induced Floquet spin-triplet Cooper pairs in unconventional magnets, *SciPost Phys.* 20(2), 059 (2026)
32. A. V. Kimel, Th. Rasing, and B. A. Ivanov, Optical readout and control of antiferromagnetic Néel vector in altermagnets and beyond, *J. Magn. Magn. Mater.* 598, 172039 (2024)
33. M. A. Reja and A. Narayan, Emergence of tunable exceptional points in altermagnet–ferromagnet junctions, *Phys. Rev. B* 110(23), 235401 (2024)
34. G. K. Dash, S. Panda, and S. Nandy, Fingerprint of non-Hermiticity in a d-wave altermagnet, *Phys. Rev. B* 111(15), 155119 (2025)
35. I. V. Maznichenko, A. Ernst, D. Maryenko, V. K. Dugaev, E. Y. Sherman, P. Buczek, S. S. P. Parkin, and S. Ostanin, Fragile altermagnetism and orbital disorder in Mott insulator $LaTiO_3$, *Phys. Rev. Mater.* 8(6), 064403 (2024)
36. X. Zhang and S. Zhang, Sliding-induced ferrovalley polarization and possible antiferromagnetic half-metal in bilayer altermagnets, *Front. Phys. (Beijing)* 21(7), 075203 (2026)
37. B. Lei, A. Li, H. Duan, M. Long, Y. Wang, and F. Ouyang, Shear-strain-induced switchable spin splitting and piezomagnetic properties in altermagnetic materials, *Front. Phys. (Beijing)* 20(6), 064204 (2025)
38. S. D. Guo, Hidden altermagnetism, *Front. Phys. (Beijing)* 21(2), 025201 (2026)
39. H. J. Lin, S. B. Zhang, H. Z. Lu, and X. C. Xie, Coulomb drag in altermagnets, *Phys. Rev. Lett.* 134(13), 136301 (2025)
40. Y. Chen, X. Liu, H. Z. Lu, and X. C. Xie, Electrical switching of altermagnetism, *Phys. Rev. Lett.* 135(1), 016701 (2025)
41. Y. Fukaya, B. Lu, K. Yada, Y. Tanaka, and J. Cayao, Crossed surface flat bands in three-dimensional superconducting altermagnets, arXiv: 2510.14724 (2025)

42. B. Lu, P. Mercebach, P. Burset, K. Yada, J. Cayao, Y. Tanaka, and Y. Fukaya, Engineering subgap states in superconductors by altermagnetism, arXiv: 2508.03364 (2025)
43. Y. Fukaya, K. Maeda, K. Yada, J. Cayao, Y. Tanaka, and B. Lu, Josephson effect and odd-frequency pairing in superconducting junctions with unconventional magnets, *Phys. Rev. B* 111(1), 064502 (2025)
44. K. Maeda, Y. Fukaya, K. Yada, B. Lu, Y. Tanaka, and J. Cayao, Classification of pair symmetries in superconductors with unconventional magnetism, *Phys. Rev. B* 111(14), 144508 (2025)
45. W. Zhao, Y. Fukaya, P. Burset, J. Cayao, Y. Tanaka, and B. Lu, Orientation-dependent transport in junctions formed by *d*-wave altermagnets and *d*-wave superconductors, *Phys. Rev. B* 111(18), 184515 (2025)
46. X. Chen, Y. Liu, P. Liu, Y. Yu, J. Ren, J. Li, A. Zhang, and Q. Liu, Unconventional magnons in collinear magnets dictated by spin space groups, *Nature* 640(8058), 349 (2025)
47. X. Chen, J. Ren, Y. Zhu, Y. Yu, A. Zhang, P. Liu, J. Li, Y. Liu, C. Li, and Q. Liu, Enumeration and representation theory of spin space groups, *Phys. Rev. X* 14(3), 031038 (2024)
48. P. Liu, J. Li, J. Han, X. Wan, and Q. Liu, Spin-group symmetry in magnetic materials with negligible spin–orbit coupling, *Phys. Rev. X* 12(2), 021016 (2022)
49. Q. Liu, X. Dai, and S. Blügel, Different facets of unconventional magnetism, *Nat. Phys.* 21(3), 329 (2025)
50. X. Duan, J. Zhang, Z. Zhu, Y. Liu, Z. Zhang, I. Žutić, and T. Zhou, Antiferroelectric altermagnets: Antiferroelectricity alters magnets, *Phys. Rev. Lett.* 134(10), 106801 (2025)
51. M. Gu, Y. Liu, H. Zhu, K. Yananose, X. Chen, Y. Hu, A. Stroppa, and Q. Liu, Ferroelectric switchable altermagnetism, *Phys. Rev. Lett.* 134(10), 106802 (2025)
52. Y. P. Zhu, X. Chen, X. R. Liu, Y. Liu, P. Liu, H. Zha, G. Qu, C. Hong, J. Li, Z. Jiang, X. M. Ma, Y. J. Hao, M. Y. Zhu, W. Liu, M. Zeng, S. Jayaram, M. Lenger, J. Ding, S. Mo, K. Tanaka, M. Arita, Z. Liu, M. Ye, D. Shen, J. Wrachtrup, Y. Huang, R. H. He, S. Qiao, Q. Liu, and C. Liu, Observation of plaid-like spin splitting in a noncoplanar antiferromagnet, *Nature* 626(7999), 523 (2024)
53. X. Yang, S. Fang, Z. Yang, P. Ho, J. Lu, and Y. S. Ang, Altermagnetic flatband-driven fermi surface geometry for giant tunneling magnetoresistance, *Adv. Funct. Mater.* 2026, e31921 (2026)
54. K. Li, Y. Hu, Y. Li, R. Xu, H. Li, K. Liu, C. Liu, J. Zhuang, Y. S. Ang, J. Wang, H. Feng, W. Hao, and Y. Du, Two-dimensional altermagnetism in epitaxial CrSb ultrathin films, arXiv: 2510.12344 (2025)
55. S. Fang, Z. Yang, J. Wang, X. Yang, J. Lu, C. H. Lee, X. Wang, and Y. S. Ang, Edgetronics in two-dimensional altermagnets, arXiv: 2508.10451 (2025)
56. R. Peng, S. Fang, P. Ho, F. Liu, T. Zhou, J. Liu, and Y. S. Ang, Ferroelastic altermagnetism, *npj Quantum Mater.* 11(1), 5 (2026)
57. L. Šmejkal, R. González-Hernández, T. Jungwirth, and J. Sinova, Crystal time-reversal symmetry breaking and spontaneous Hall effect in collinear antiferromagnets, *Sci. Adv.* 6(23), eaaz8809 (2020)
58. N. J. Ghimire, A. S. Botana, J. S. Jiang, J. Zhang, Y. S. Chen, and J. F. Mitchell, Large anomalous Hall effect in the chiral-lattice antiferromagnet $CoNb_3S_6$, *Nat. Commun.* 9(1), 3280 (2018)
59. X. Zhou, W. Feng, R. W. Zhang, L. Šmejkal, J. Sinova, Y. Mokrousov, and Y. Yao, Crystal thermal transport in altermagnetic RuO_2, *Phys. Rev. Lett.* 132(5), 056701 (2024)
60. R. D. Gonzalez Betancourt, J. Zubáň, R. Gonzalez-Hernandez, K. Geishendorf, Z. Šobáň, G. Springholz, K. Olejn'ık, L. Šmejkal, J. Sinova, T. Jungwirth, S. T. B. Goennenwein, A. Thomas, H. Reichlová, J. Šelezn' y, and D. Kriegner, Spontaneous anomalous Hall effect arising from an unconventional compensated magnetic phase in a semiconductor, *Phys. Rev. Lett.* 130(3), 036702 (2023)
61. M. Leiviskä, J. Rial, A. Bad'ura, R. L. Seeger, I. Kounta, S. Beckert, D. Kriegner, I. Joumard, E. Schmoranzerova, J. Sinova, O. Gomonay, A. Thomas, S. T. B. Goennenwein, H. Reichlová, L. Šmejkal, L. Michez, T. Jungwirth, and V. Baltz, Anisotropy of the anomalous Hall effect in thin films of the altermagnet candidate Mn_5Si_3, *Phys. Rev. B* 109(22), 224430 (2024)
62. A. Fakhredine, R. M. Sattigeri, G. Cuono, and C. Autieri, Interplay between altermagnetism and nonsymmorphic symmetries generating large anomalous Hall conductivity by semi-Dirac points induced anticrossings, *Phys. Rev. B* 108(11), 115138 (2023)
63. X. Y. Hou, H. C. Yang, Z. X. Liu, P. J. Guo, and Z. Y. Lu, Large intrinsic anomalous Hall effect in both Nb_2FeB_2 and Ta_2FeB_2 with collinear antiferromagnetism, *Phys. Rev. B* 107(16), L161109 (2023)
64. T. P. T. Nguyen and K. Yamauchi, Ab initio prediction of anomalous Hall effect in antiferromagnetic $CaCrO_3$, *Phys. Rev. B* 107(15), 155126 (2023)
65. M. Naka, Y. Motome, and H. Seo, Anomalous Hall effect in antiferromagnetic perovskites, *Phys. Rev. B* 106(19), 195149 (2022)
66. H. Y. Ma, M. Hu, N. Li, J. Liu, W. Yao, J. F. Jia, and J. Liu, Multifunctional antiferromagnetic materials with giant piezomagnetism and noncollinear spin current, *Nat. Commun.* 12(1), 2846 (2021)
67. R. González-Hernández, L. Šmejkal, K. Výborný, Y. Yahagi, J. Sinova, T. Jungwirth, and J. Železný, Efficient electrical spin splitter based on nonrelativistic collinear antiferromagnetism, *Phys. Rev. Lett.* 126(12), 127701 (2021)
68. M. Naka, S. Hayami, H. Kusunose, Y. Yanagi, Y. Motome, and H. Seo, Spin current generation in organic antiferromagnets, *Nat. Commun.* 10(1), 4305 (2019)
69. M. Naka, Y. Motome, and H. Seo, Perovskite as a spin current generator, *Phys. Rev. B* 103(12), 125114 (2021)
70. H. Bai, Y. C. Zhang, Y. J. Zhou, P. Chen, C. H. Wan, L. Han, W. X. Zhu, S. X. Liang, Y. C. Su, X. F. Han, F. Pan, and C. Song, Efficient spin-to-charge conversion via altermagnetic spin splitting effect in antiferromagnet RuO_2, *Phys. Rev. Lett.* 130(21), 216701 (2023)
71. Q. Cui, Y. Zhu, X. Yao, P. Cui, and H. Yang, Giant

spin-Hall and tunneling magnetoresistance effects based on a two-dimensional nonrelativistic antiferromagnetic metal, *Phys. Rev. B* 108(2), 024410 (2023)
72. M. Ezawa, Third-order and fifth-order nonlinear spin-current generation in *g*-wave and *i*-wave altermagnets and perfectly nonreciprocal spin current in *f*-wave magnets, *Phys. Rev. B* 111(12), 125420 (2025)
73. N. Wang, J. Chen, N. Ding, H. Zhang, S. Dong, and S. S. Wang, Magneto-optical Kerr effect and magnetoelasticity in a weakly ferromagnetic RuF_4 monolayer, *Phys. Rev. B* 106(6), 064435 (2022)
74. I. Gray, Q. Deng, Q. Tian, M. Chilcote, J. Dodge, M. Brahlek, and L. Wu, Time-resolved magneto-optical effects in the altermagnet candidate MnTe, *Appl. Phys. Lett.* 125(21), 212404 (2024)
75. A. Hariki, A. Dal Din, O. J. Amin, T. Yamaguchi, A. Badura, D. Kriegner, K. W. Edmonds, R. P. Campion, P. Wadley, D. Backes, L. S. I. Veiga, S. S. Dhesi, G. Springholz, L. Šmejkal, K. Vyborny, T. Jungwirth, and J. Kuneš, X-ray magnetic circular dichroism in altermagnetic *α*-MnTe, *Phys. Rev. Lett.* 132(17), 176701 (2024)
76. X. Zhou, W. Feng, X. Yang, G. Y. Guo, and Y. Yao, Crystal chirality magneto-optical effects in collinear antiferromagnets, *Phys. Rev. B* 104(2), 024401 (2021)
77. A. Hariki, Y. Takahashi, and J. Kuneš, X-ray magnetic circular dichroism in RuO_2, *Phys. Rev. B* 109(9), 094413 (2024)
78. P. Kesler, L. Garcia-Gassull, A. Suter, T. Prokscha, Z. Salman, D. Khalyavin, P. Manuel, F. Orlandi, I. I. Mazin, R. Valentí, and S. Moser, Absence of magnetic order in RuO_2: Insights from μSR spectroscopy and neutron diffraction, *npj Spintronics* 2(1), 50 (2024)
79. B. Z. Gregory, N. Wadehra, S. Zhang, Y. Wu, S. Poage, J. Strempfer, A. K. Kundu, A. Rajapitamahuni, E. Vescovo, A. Verma, B. Pamuk, J. Ruf, H. Nair, N. J. Schreiber, K. Ahadi, K. M. Shen, D. G. Schlom, and A. Singer, Resonant diffraction and photoemission inconsistent with altermagnetism in epitaxial RuO_2 films, arXiv: 2510.13781 (2025)
80. J. Liu, J. Zhan, T. Li, J. Liu, S. Cheng, Y. Shi, L. Deng, M. Zhang, C. Li, J. Ding, Q. Jiang, M. Ye, Z. Liu, Z. Jiang, S. Wang, Q. Li, Y. Xie, Y. Wang, S. Qiao, J. Wen, Y. Sun, and D. Shen, Absence of altermagnetic spin splitting character in rutile oxide RuO_2, *Phys. Rev. Lett.* 133(17), 176401 (2024)
81. A. A. Tsirlin, E. Uykur, and O. Janson, Is ruthenium dioxide altermagnet? arXiv: 2511.01647 (2025)
82. V. Galitski and I. B. Spielman, Spin–orbit coupling in quantum gases, *Nature* 494(7435), 49 (2013)
83. A. Manchon, H. C. Koo, J. Nitta, S. M. Frolov, and R. A. Duine, New perspectives for Rashba spin–orbit coupling, *Nat. Mater.* 14(9), 871 (2015)
84. Z. Y. Zhuang, D. Zhu, D. Liu, Z. Wu, and Z. Yan, Odd-parity altermagnetism originated from orbital orders, arXiv: 2508.18361 (2025)
85. C. Lee, N. A. Hackner, and P. M. R. Brydon, Incommensuration in odd–parity magnets, *Phys. Rev. B* 113(6), 064420 (2026)
86. E. W. Hodt, H. Bentmann, and J. Linder, Fate of *p*-wave spin polarization in helimagnets with Rashba spin–orbit coupling, *Phys. Rev. B* 111(20), 205416 (2025)
87. M. Ezawa, Planar Hall effects in *X*-wave magnets with $X = p; d; g; f; i$, arXiv: 2508.09472 (2025)
88. H. Zhou, M. Wang, X. Ma, G. Li, D. F. Shao, B. Liu, and S. Li, Anisotropic resistivity of a *p*-wave magnet candidate CeNiAsO, arXiv: 2509.07351 (2025)
89. T. Kokkeler, I. Tokatly, and F. S. Bergeret, Quantum transport theory for unconventional magnets: Interplay of altermagnetism and *p*-wave magnetism with superconductivity, *SciPost Phys.* 18(6), 178 (2025)
90. A. Chakraborty, A. Birk Hellenes, R. Jaeschke-Ubiergo, T. Jungwirth, L. Šmejkal, and J. Sinova, Highly efficient non-relativistic Edelstein effect in nodal p-wave magnets, *Nat. Commun.* 16(1), 7270 (2025)
91. M. Ezawa, Tunneling magnetoresistance in a junction made of *X*-wave magnets with $X = p; d; f; g; i$, arXiv: 2509.16867 (2025)
92. S. Das and A. Soori, Orientation dependent anomalous Hall and spin Hall currents at junctions of altermagnets with *p*-wave magnets, *Phys. Rev. B* 112(23), 235309 (2025)
93. M. A. Reja and A. Narayan, Néel vector controlled exceptional contours in p-wave magnet-ferromagnet junctions, *New J. Phys.* 27(9), 092001 (2025)
94. M. Alipourzadeh, D. Afshar, and Y. Hajati, Opto- and magneto-tunable exceptional degeneracies in non-Hermitian ferromagnet/*p*-wave magnet junctions, arXiv: 2508.01295 (2025)
95. W. Zeng, Tunneling spin Hall effect induced by unconventional *p*-wave magnetism, *Phys. Rev. B* 112(14), 144516 (2025)
96. M. Salehi, Transverse spin supercurrent at *p*-wave magnetic Josephson junctions, arXiv: 2507.11397 (2025)
97. Y. Fukaya, K. Yada, and Y. Tanaka, Tunneling conductance in superconducting junctions with p-wave unconventional magnets breaking time-reversal symmetry, *J. Supercond. Nov. Magn.* 38(6), 228 (2025)
98. K. Maeda, B. Lu, K. Yada, and Y. Tanaka, Theory of tunneling spectroscopy in unconventional *p*-wave magnet-superconductor hybrid structures, *J. Phys. Soc. Jpn.* 93(11), 114703 (2024)
99. P. Sukhachov, H. G. Giil, B. Brekke, and J. Linder, Coexistence of *p*-wave magnetism and superconductivity, *Phys. Rev. B* 111(22), L220403 (2025)
100. A. Soori, Crossed Andreev reflection in collinear *p*-wave magnet/triplet superconductor junctions, *Phys. Rev. B* 111(16), 165413 (2025)
101. S. Hong, M. J. Park, and K. M. Kim, Unconventional *p*-wave and finite-momentum superconductivity induced by altermagnetism through the formation of Bogoliubov Fermi surface, *Phys. Rev. B* 111(5), 054501 (2025)
102. Q. Song, S. Stavrić, P. Barone, A. Droghetti, D. S. Antonenko, J. W. F. Venderbos, C. A. Occhialini, B. Ilyas, E. Ergeçen, N. Gedik, S. W. Cheong, R. M. Fernandes, S. Picozzi, and R. Comin, Electrical switching of a p-wave magnet, *Nature* 642(8066), 64 (2025)
103. R. Yamada, M. T. Birch, P. R. Baral, S. Okumura, R.

Nakano, S. Gao, M. Ezawa, T. Nomoto, J. Masell, Y. Ishihara, K. K. Kolincio, I. Belopolski, H. Sagayama, H. Nakao, K. Ohishi, T. Ohhara, R. Kiyanagi, T. Nakajima, Y. Tokura, T. Arima, Y. Motome, M. M. Hirschmann, and M. Hirschberger, A metallic p-wave magnet with commensurate spin helix, *Nature* 646(8086), 837 (2025)

104. M. Ezawa, Purely electrical detection of the spin-splitting vector in p-wave magnets based on linear and nonlinear conductivities, *Phys. Rev. B* 112(12), 125412 (2025)
105. M. Ezawa, Quantum geometry and elliptic optical dichroism in p-wave magnets, *Phys. Rev. B* 112(4), 045302 (2025)
106. A. Dal Din, O. J. Amin, P. Wadley, and K. W. Edmonds, Antiferromagnetic spintronics and beyond, *npj Spintronics* 2(1), 25 (2024)
107. A. Hirohata, K. Yamada, Y. Nakatani, I. L. Prejbeanu, B. Diény, P. Pirro, and B. Hillebrands, Review on spintronics: Principles and device applications, *J. Magn. Magn. Mater.* 509, 166711 (2020)
108. M. Ciorga, Perspective on the spin field-effect transistor, *J. Phys. D Appl. Phys.* 58(1), 012001 (2025)
109. S. Bandyopadhyay and M. Cahay, Reexamination of some spintronic field-effect device concepts, *Appl. Phys. Lett.* 85(8), 1433 (2004)
110. S. Jiang, L. Li, Z. Wang, J. Shan, and K. F. Mak, Spin tunnel field-effect transistors based on two-dimensional van der Waals heterostructures, *Nat. Electron.* 2(4), 159 (2019)
111. S. Datta and B. Das, Electronic analog of the electro-optic modulator, *Appl. Phys. Lett.* 56(7), 665 (1990)
112. S. Datta, Electronic Transport in Mesoscopic Systems, Cambridge, Cambridge University Press, 1995
113. B. K. Nikolić, L. P. Zârbo, and S. Souma, Imaging mesoscopic spin Hall flow: Spatial distribution of local spin currents and spin densities in and out of multiterminal spin-orbit coupled semiconductor nanostructures, *Phys. Rev. B* 73(7), 075303 (2006)
114. A. P. Jauho, Nonequilibrium Green function modelling of transport in mesoscopic systems, in: Progress in Nonequilibrium Green's Functions II, World Scientific, 2003, pp 181–197
115. H. Haug and A. P. Jauho, Quantum Kinetics in Transport and Optics of Semiconductors, 2nd Ed. , Springer, Berlin, Heidelberg, 2008
116. P. H. Fu, Y. Xu, X. L. Yu, J. F. Liu, and J. Wu, Electrically modulated Josephson junction of light-dressed topological insulators, *Phys. Rev. B* 105(6), 064503 (2022)